Substituent Effects on Non-Covalent Bonds: Complexes of Ionized Benzene Derivatives with Hydrogen Cyanide.

ARTICLE *in* THE JOURNAL OF PHYSICAL CHEMISTRY A · SEPTEMBER 2013

Impact Factor: 2.69 · DOI: 10.1021/jp4069202 · Source: PubMed

6 AUTHORS, INCLUDING:

Ahmed Hamid
Pacific Northwest National Laboratory
24 PUBLICATIONS **91** CITATIONS
SEE PROFILE

Michael Noah Mautner
Virginia Commonwealth University
198 PUBLICATIONS **5,132** CITATIONS
SEE PROFILE

M. Samy El-Shall
Virginia Commonwealth University
272 PUBLICATIONS **4,519** CITATIONS
SEE PROFILE

Abdulrahman Al-youbi
King Abdulaziz University
223 PUBLICATIONS **2,493** CITATIONS
SEE PROFILE

THE JOURNAL OF PHYSICAL CHEMISTRY A

Article

pubs.acs.org/JPCA

Substituent Effects on Noncovalent Bonds: Complexes of Ionized Benzene Derivatives with Hydrogen Cyanide

Isaac K. Attah, Ahmed M. Hamid, Michael Meot-Ner (Mautner), and M. S. El-Shall*

Department of Chemistry, Virginia Commonwealth University, Richmond, Virginia 23284-2006, United States

Saadullah G. Aziz and Abdulrahman O. Alyoubi

Department of Chemistry, Faculty of Science, King Abdulaziz University, Jeddah 21589, Saudi Arabia

Supporting Information

ABSTRACT: Here, we report the first experimental and computational study of the noncovalent binding energies and structures of ionized benzenes containing electron-withdrawing substituents solvated by one to four HCN molecules. Measured by ion mobility mass spectrometric equilibrium studies, the bond dissociation enthalpies of the first HCN molecule to the fluorobenzene ($C_6H_5F^{\bullet+}$), 1,4-difluorobenzene ($C_6H_4F_2^{\bullet+}$), and benzonitrile ($C_6H_5CN^{\bullet+}$) ions (11.2, 11.2, and 9.2 kcal/mol, respectively) are similar to those of HCN with the benzene ($C_6H_6^{\bullet+}$) and phenyacetylene ($C_6H_5CCH^{\bullet+}$) radical cations (9.2 and 10.5 kcal/mol, respectively). DFT calculations at the B3LYP/6-311++G(d,p) level show that HCN can form in-plane hydrogen bonds to ring hydrogens, or bind electrostatically to positively charged carbon centers in the ring. The electron-withdrawing substituents increase the bond energy by increasing the partial positive charge on the ring hydrogens that form $CH^{\delta+}$---NCH bonds, and by creating a π hole, as evidenced by positive charge centers on the fluorinated ring carbons for electrostatically bonded isomers. In the complexes of benzonitrile$^{\bullet+}$, similar to benzene$^{\bullet+}$, hydrogen bonded planar isomers have the lowest energy. In the complexes of (fluorinated benzene)$^{\bullet+}$, the lowest energy isomers are electrostatically bonded where HCN is perpendicular to the ring and its dipole points to a positively charged ring carbon. However, in all cases the planar hydrogen-bonded and vertical electrostatic isomers have similar binding energies within 1 kcal/mol, although HCN interacts with different sites of the ionized benzenes in these isomers, suggesting that the observed cluster populations are mixtures of the planar and vertical isomers. Further HCN molecules can bind directly to unoccupied ring CH hydrogens or bind to the first-shell HCN molecules to form linear HCN---HCN--- hydrogen bonded chains. The binding energies decrease stepwise to about 6−7 kcal/mol by 4 HCN molecules, approaching the macroscopic enthalpy of vaporization of liquid HCN (6.0 kcal/mol).

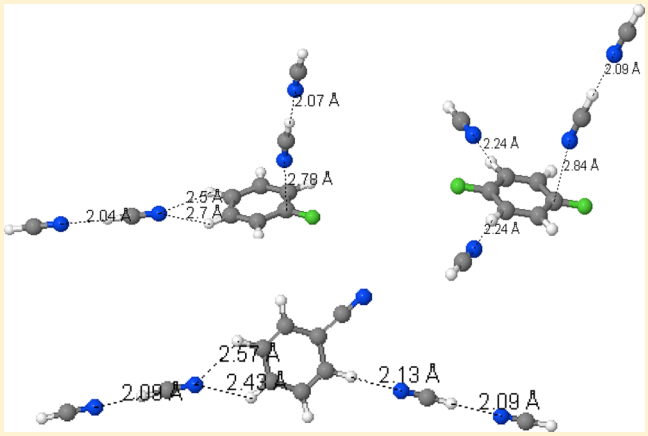

1. INTRODUCTION

Intermolecular forces, including hydrogen bonds,[1−4] are important in chemical synthesis, crystal and materials engineering, molecular recognition and supramolecular chemistry, polymerization, biology, and astrochemistry.[5−14] Ionic hydrogen bonds are strong intermolecular forces, often 10−30 kcal/mol, which can form in ionizing environments between radical ions or protonated molecules and neutral molecules. Such bonds can form between stable molecular ions of aromatic hydrocarbons and polar solvent molecules. It is of interest how substituents on the molecular ions affect these intermolecular forces. These effects can be studied experimentally by measuring ion−molecule binding energies, and computationally by calculating the binding energies, structures, and charge distributions of the complexes.

Ion−neutral complexes involving ionized aromatics such as benzene$^{\bullet+}$ can form three types of structures: (1) parallel sandwich type π stacked complexes with neutral aromatic molecules, (2) planar hydrogen-bonded, or (3) vertical electrostatic complexes with polar ligands. The present study investigates substituent effects on the hydrogen bonded and electrostatic isomers of the complexes formed by stepwise solvation of ionized benzene derivatives and one to four HCN molecules.

Early studies addressed substituent effects on noncovalent sandwich type complexes in $(benzene)_2^{\bullet+}$ and similar dimers of

Received: July 12, 2013
Revised: September 9, 2013
Published: September 11, 2013

benzene derivatives and polycyclic aromatic hydrocarbons.[15−20] These dimers usually have parallel π stacked sandwich structures where the positive charge is delocalized between the fragments as required by symmetry in sandwich structures which allow charge transfer (CT) resonance between the components.[16,20−22] This is most effective in homodimers with sandwich structures, contributing 6−7 kcal/mol of the 17 kcal/mol binding energy in $(benzene)_2^{\bullet+}$.[16,20−22] However, CT becomes weaker in heterodimers where the charge is localized on the component with the lower ionization energy. Pieniazek et al.[23,24] characterized the electronic structure of the ten lowest ionized states of the neutral benzene dimer which has two nearly isoenergetic isomers: a T-shaped and a displaced sandwich isomer.[23−26] They found that relaxation along the intermolecular distance and sliding displacements, in addition to Jahn−Teller distortions lower the energy of the displaced sandwich isomer significantly more than of the T-shaped isomer.[23,24] Interestingly, a considerable delocalization of the positive charge is found in the T-shaped benzene dimer cation that can result in CT resonance bands in the spectrum.[23,24] Substituent groups that affect the ionization energies can thereby affect the bond energies and the extent of charge delocalization in symmetry-broken dimer configurations.[16,18−24]

Alternatively, hydrogen bonded adducts form with nonaromatic polar molecules such as H_2O, HCN, and CH_3CN, which bound to $benzene^{\bullet+}$ or other ionized aromatics through $-CH^{\delta+}$---O or $-CH^{\delta+}$---N hydrogen bonds.[27−33] Additional solvent molecules can then bind to other unoccupied benzene CH hydrogens, forming internally solvated structures (with the ion inside a solvent cluster), or attach to the first solvent molecule forming an externally solvated cluster (with the ion outside the solvent cluster). Solvation by three or more solvent molecules can also form mixtures of both internally and externally solvated structures.[27−33] In these cases substituents on the ionized aromatic molecule can affect the charge densities on the ring carbons and on the CH hydrogens and thereby affect the ionic hydrogen bonds.

In addition to the sandwich and hydrogen-bonded adducts, a third type of structure is observed in some cases, where ligand molecules bound electrostatically to charge centers in the ionized aromatics. We found thermochemical indications for such electrostatic complexes in adducts of polar ligands such as CH_3CN and CH_3NO_2 to $aniline^{\bullet+}$.[18] In some cases the thermochemistry indicates that electrostatic complexes are more stable than possible π stacked sandwich complexes, such as in $aniline^{\bullet+}$−benzonitrile or $aniline^{\bullet+}$−nitrobenzene[18,20] or in noncovalent noncoplanar isomers of the $benzene^{\bullet+}$−pyridine dimer, where the pyridine N atom points to a partial charge on a benzene carbon in the ring.[34] However, there is little information on the effects of ring substituents on the intermolecular interactions of ionized aromatics. The present work examines the effects of electron-withdrawing substituents on benzene in complexes of ionized fluorobenzenes and benzonitrile with one to four HCN molecules.

Hydrogen cyanide is a useful probe of noncovalent interactions because it is highly polar, and it can serve both as a hydrogen donor and as a lone-pair hydrogen acceptor in hydrogen bonds. We recently studied the stepwise association of HCN with phenylacetylene and benzene radical cations.[32,33] In $benzene^{\bullet+}(HCN)_n$ clusters the ligand molecules are bonded to the benzene hydrogens by $-CH^{\delta+}$---N hydrogen bonds, but linear hydrogen bonded HCN---HCN---HCN chains are also formed with further HCN molecules.[33] In the $phenylacetylene^{\bullet+}(HCN)_n$ clusters, the dominant interaction was hydrogen bonding between the C−H acetylene hydrogen and the nitrogen atom of the first HCN ligand.[32] Here also subsequent ligand molecules are added to form linear hydrogen bonded $phenylacetylene^{\bullet+}$(NCH---NCH---) chains.[32] Such chains were indicated previously in protonated $(HCN)_nH^+$ clusters HCN---(HCN---(HCN---H^+---NCH)---NCH)---NCH where binding enthalpies indicated completion of solvent shells by two (first shell) or four (second shell) HCN molecules about the proton.[1,35,36]

In the present paper we report the sequential binding energies of one to four HCN molecules to substituted ionized benzenes (fluorobenzene, 1,4-difluorobenzene and benzonitrile), and we use computational chemistry to investigate the types of hydrogen bonds and their relative stabilities in these clusters.

2. EXPERIMENTAL AND THEORETICAL METHODS

The ion association experiments reported here are carried out using the VCU mass-selected ion mobility mass spectrometer. Details of the instrument are given elsewhere.[21,22,28,31,33] To generate the molecular radical cations $C_6H_5F^{\bullet+}$, $C_6H_4F_2^{\bullet+}$, and $C_7H_5N^{\bullet+}$, the neutral monomers are generated by the supersonic expansion of 40 psi (2.7 atm) of ultrahigh pure helium seeded with about 1−4% of vapor of the corresponding compound (fluorobenzene, 1,4-difluorobenzene, and benzonitrile, respectively) through a pulsed supersonic nozzle (500 μm) to the vacuum source chamber with 10^{-7} Torr pressure and are ionized by electron impact ionization using an electron energy of 60−70 eV. The radical cations are then mass selected using the first quadrupole mass filter and injected in 30−50 μs pulses into the drift cell, which contains HCN vapor in a helium buffer gas mixture.

To allow a known and constant concentration of HCN and helium pressure into the drift cell, two flow controllers (MKS # 1479 accurate within ±1 mTorr) are used. The drift cell temperature is controlled within ±1 K using four temperature controllers. Liquid nitrogen flow, controlled using electronic solenoid valves is used to cool down the drift cell. The second quadrupole mass filter is used to scan and detect the product distribution from the reaction after exiting the drift cell. The arrival time distributions (ATDs) are collected by monitoring the intensity of each ion as a function of reaction time, and to vary the reaction time, the drift cell voltage is varied to change the drift time accordingly.

The ions are injected into the mobility cell with injection energies of 8−14 eV, laboratory frame, just above the minimum energies required to introduce the ions into the cell against the backward flow of the HCN/He mixture from the drift cell entrance orifice. Most of the thermalization of the injected ion occurs just outside the cell entrance by collisions with the HCN molecules and He atoms escaping from the cell. Further thermalization occurs in the mobility cell. For example, at a given cell pressure of 0.8 Torr at 300 K, ions undergo over 10^4 collisions with neutral molecules at >1 ms residence time inside the cell, which is more than sufficient for efficient thermalization of the ions.[31,33]

The HCN vapor used in our experiment is prepared by adding 8 g of sodium cyanide (NaCN) (Sigma-Aldrich, 97%) into a 500 mL stainless steel bubbler, which is then placed in liquid nitrogen and evacuated. Four milliliters of pure sulfuric acid (H_2SO_4) (Aldrich, 99.999%) is then added through a

dx.doi.org/10.1021/jp4069202 | J. Phys. Chem. A 2013, 117, 10588−10597

stainless steel tube extension of the inlet valve of the bubbler. To generate the HCN gas, the temperature of the stainless steel bubbler is allowed to increase to room temperature, by which time the reaction of sulfuric acid with the sodium cyanide salt inside the bubbler will occur. To ensure safety, the pressure of HCN in the closed circuit line is constantly monitored using a Baratron pressure gauge (MKS-26A13TBD) to ensure there is no leakage. Equation 1 represents the equilibrium reactions being measured during this study.

$$A^{\bullet+}(HCN)_{n-1} + HCN \rightleftharpoons A^{\bullet+}(HCN)_n \quad (1)$$

where $A^{\bullet+} = C_6H_5F^{\bullet+}$, $C_6H_4F_2^{\bullet+}$, or $C_6H_5CN^{\bullet+}$. The check for the attainment of equilibrium is done by ensuring that the following conditions are satisfied: (i) a constant ratio of the integrated intensity of the product to the reactant ions obtained during the residence time of the ions in the cell and (ii) the ATDs of the reactant and product ions are similar indicating that the product and reactant ions in the equilibrium are coupled reactively faster than their movement through the cell. After equilibrium conditions have been established, the equilibrium constant, K_{eq}, can be measured using eq 2.

$$K_{eq} = I[A^{\bullet+}(HCN)_n]/[I(A^{\bullet+}(HCN)_{n-1})(P_{HCN})] \quad (2)$$

Here $I[A^{\bullet+}(HCN)_{n-1}]$ and $I[A^{\bullet+}(HCN)_n]$ are the integrated signal intensities of the ATDs of the reactant and product ions, respectively, and P_{HCN} is the pressure of HCN in the reaction cell in atmospheres. The equilibrium constant, K_{eq}, is obtained at different temperatures, and the thermodynamic quantities ΔH° and ΔS° are obtained from the slope and intercept, respectively, of the van't Hoff plot. All values measured in this experiment were replicated at least three times, and the average values are shown in Tables 1−3 with their corresponding uncertainties.

Density functional theory (DFT) calculations of the lowest energy geometries for the various isomers of the cluster ions $A^{\bullet+}(HCN)_n$ [$A^{\bullet+} = C_6H_5F^{\bullet+}$, $C_6H_4F_2^{\bullet+}$, or $C_6H_5CN^{\bullet+}$] were performed at the B3LYP/6-311++G(d,p) level of theory using the Gaussian 03 program suite.[37] Vibrational frequency calculations were also performed for all the optimized geometries at the same level of theory to obtain zero point vibrational energy (ZPVE) and also to verify the absence of any imaginary frequencies.[37] The sequential binding energy of the $A^{\bullet+}(HCN)_n$ cluster ($\Delta E_{n-1,n}$) was calculated according to:

$$\Delta E_{n-1,n} = E(A^{\bullet+}(HCN)_{n-1}) + E(HCN) - E(A^{\bullet+}(HCN)_n) \quad (3)$$

No corrections to BSSE were made to the calculated binding energies because previous studies on related systems showed these corrections to be very small (0.1−0.4 kcal/mol).[32,33]

3. MASS SPECTRA AND ARRIVAL TIMES DISTRIBUTIONS

Figure 1a shows the mass spectrum collected following the injection of mass selected fluorobenzene radical cation into the drift cell containing 0.598 Torr helium at 300 K. This spectrum shows that there are no dissociation products of the $C_6H_5F^{\bullet+}$ ion, due to the low injection energy used in our study (13.1 eV, laboratory frame), which allows the ions to enter the drift cell against the backflow of the helium gas escaping through the orifice. Parts b−e of Figure 1 show the mass spectra obtained when the $C_6H_5F^{\bullet+}$ ion is injected into the drift cell containing HCN vapor in helium at different temperatures as indicated.

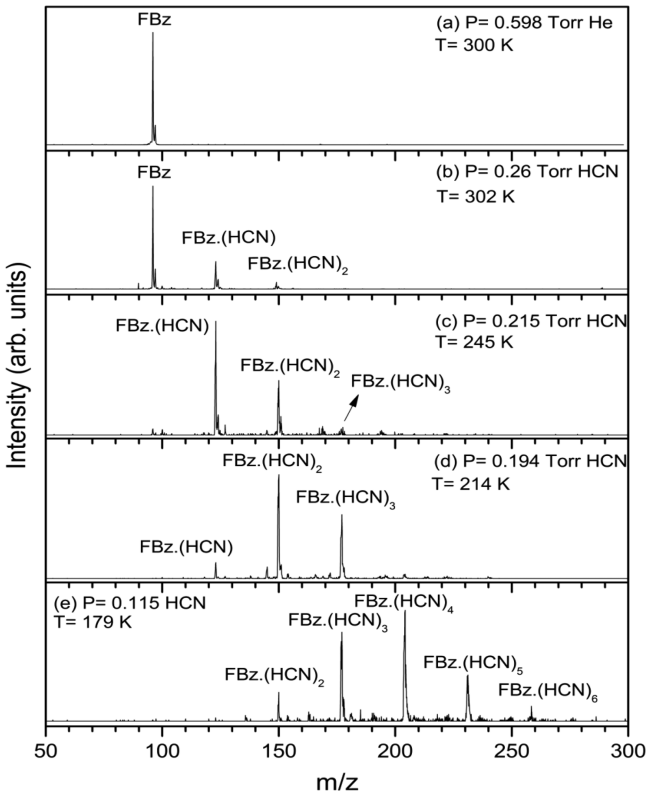

Figure 1. Mass spectra obtained following the injection of the mass-selected $C_6H_5F^{\bullet+}$ (FBz) into the drift cell containing He or HCN vapor at different pressures and temperatures as indicated.

The intensity of the $C_6H_5F^{\bullet+}$ ion signal is observed to disappear as the temperature decreases and the equilibrium shifts to the higher addition products of $C_6H_5F^{\bullet+}(HCN)_n$, as shown in Figure 1c−e. The mass spectrum shown in Figure 1e was collected with 0.115 Torr HCN at 179 K, the lowest temperature we were able to attain before HCN vapor froze in the cell. Under these conditions we observed $C_6H_5F^{\bullet+}(HCN)_4$ as the most abundant cluster among the $C_6H_5F^{\bullet+}(HCN)_n$ clusters' distribution with $n = 1-6$.

To verify equilibrium, we collected ATD's for the $C_6H_5F^{\bullet+}(HCN)_{n-1}$, $C_6H_5F^{\bullet+}(HCN)_n$, and $C_6H_5F^{\bullet+}(HCN)_{n+1}$ ions. In principle, reactant and product ions coupled by equilibrium in an association reaction will have similar ATDs, due to the fact that, for example, $C_6H_5F^{\bullet+}(HCN)_{n-1}$ will exist in a fixed ratio with respect to $C_6H_5F^{\bullet+}(HCN)_n$ and the equilibrium between them switches back and forth faster than the drift of the ions in the cell. Figure 2 shows the overlapping of the ATDs of $C_6H_5F^{\bullet+}(HCN)_n$, with $n = 0-4$, indicating that the ions are under equilibrium conditions. The small differences in the maxima of the ATD peaks are due to the differences in the masses of the reactant and product ions.

Figure 3 shows the mass spectra for the 1,4-difluorobenzene$^{\bullet+}$/HCN clusters obtained by methods similar to those described for the fluorobenzene$^{\bullet+}$/HCN system, at 300 K (Figure 3b), 259 K (Figure 3c), and 219 K (Figure 3d). A similar shifting trend in the cluster distribution toward higher clusters is observed at low temperatures, with up to six HCN molecules observed at 159 K (not shown). The ATDs were also collected at 269 and 208 K and showed overlap similar to the ATDs shown in Figure 2 for the fluorobenzene$^{\bullet+}$/HCN system.

dx.doi.org/10.1021/jp4069202 | J. Phys. Chem. A 2013, 117, 10588−10597

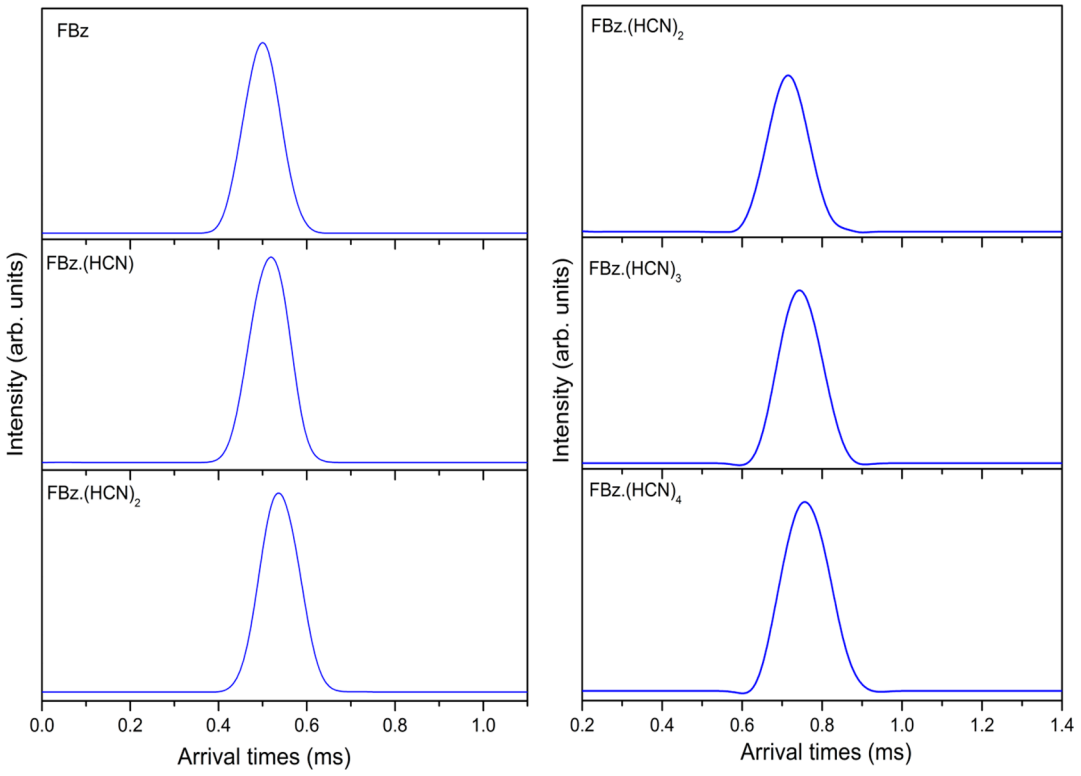

Figure 2. Arrival time distributions of the $C_6H_5F^{\bullet+}(HCN)_n$ ions with $n = 0-2$ obtained following the injection of mass selected fluorobenzene ions into 0.2 Torr of HCN vapor at 263 K (left) and at 203 K for $n = 2-4$ (right).

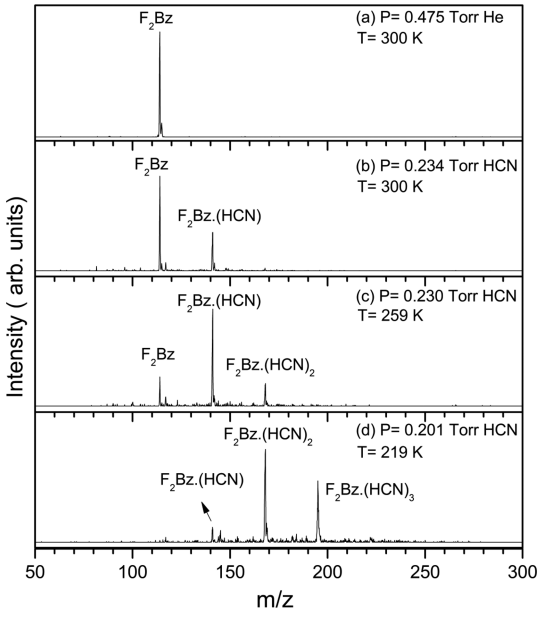

Figure 3. Mass spectra obtained following the injection of the mass-selected 1,4-difluorobenzene cation ($C_6H_4F_2^{\bullet+}$ (F_2Bz)) into the drift cell containing He or HCN vapor at different pressures and temperatures as indicated.

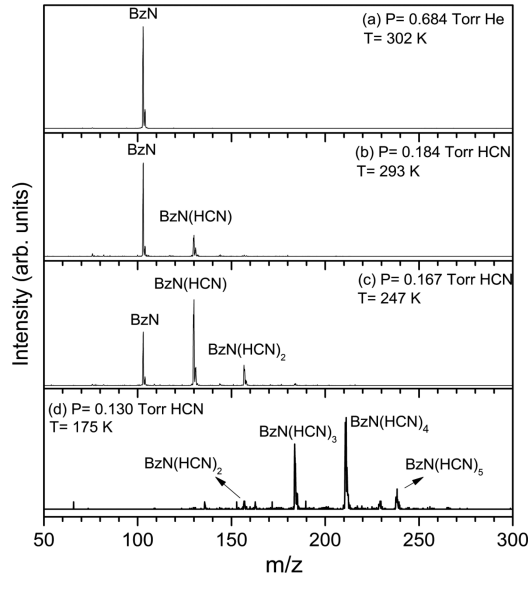

Figure 4. Mass spectra obtained following the injection of the mass-selected $C_6H_5CN^{\bullet+}$ (BzN) ions into the drift cell containing He and HCN vapor at different pressures and temperatures as indicated.

Similar to the above studies, Figure 4a shows the mass spectrum of mass-selected benzonitrile radical cation injected into 0.684 Torr pure helium at 302 K. Parts b–d of Figure 4 show the mass spectra of the $C_6H_5CN^{\bullet+}$/HCN system obtained by injecting the mass selected $C_6H_5CN^{\bullet+}$ into the drift cell containing HCN vapor at different temperatures. Again, as the temperature of the drift cell is lowered, the equilibrium conditions tend to favor the higher $C_6H_5CN^{\bullet+}(HCN)_n$ cluster ions, with gradual diminishing and eventual disappearance of the $C_6H_5CN^{\bullet+}$ ion. The ATDs of the $C_6H_5CN^{\bullet+}$ $(HCN)_n$ ions also overlapped giving further evidence for the attainment of equilibrium conditions.

dx.doi.org/10.1021/jp4069202 | J. Phys. Chem. A 2013, 117, 10588–10597

4. THERMOCHEMISTRY, BINDING ENERGIES, AND STRUCTURES

The measured equilibrium constants yielded the van't Hoff plots shown in Figures 5−7, and the thermochemical ΔH° and

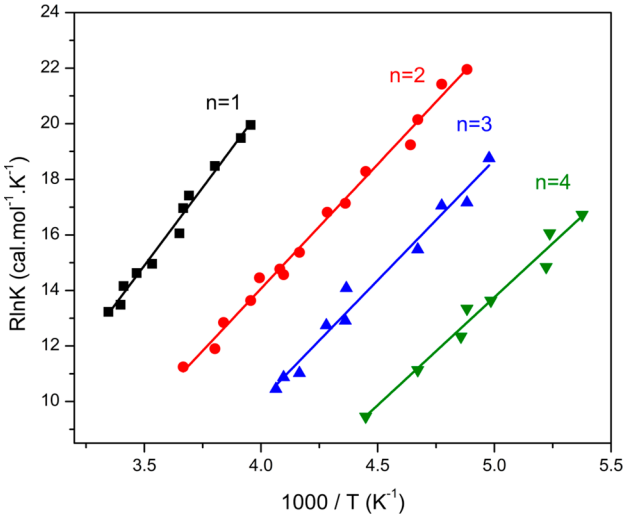

Figure 5. van't Hoff plots for the $C_6H_5F^{\bullet+}(HCN)_{n-1}$ + HCN ⇌ $C_6H_5F^{\bullet+}(HCN)_n$ association reactions for n = 1−4 as indicated.

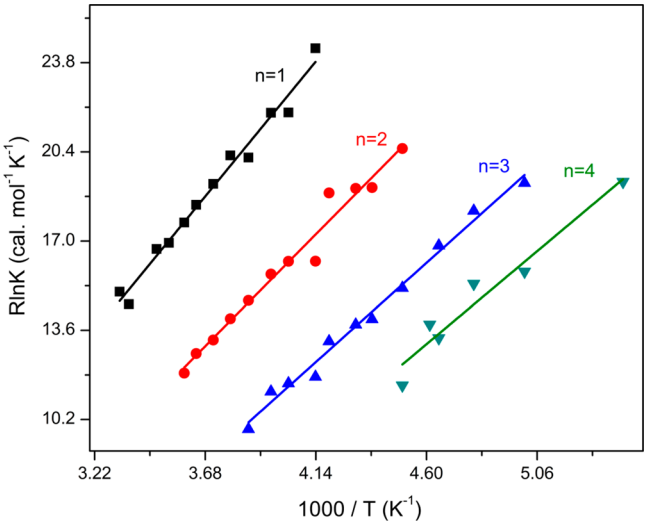

Figure 6. van't Hoff plots for the $C_6H_4F_2^{\bullet+}(HCN)_{n-1}$ + HCN ⇌ $C_6H_4F_2^{\bullet+}(HCN)_n$ association reactions for n = 1−4 as indicated.

ΔS° values are reported in Tables 1−3 along with the DFT binding energies (ΔE) calculated at the B3LYP/6-311++G(d, p) level. For all the ions, we were able to measure the ΔH° and ΔS° for up to the fourth addition, i.e., $\Delta H^\circ_{3,4}$ and $\Delta S^\circ_{3,4}$. Comparisons of the measured ΔH° of one to four HCN molecules to the present ions and to the benzene ($C_6H_6^{\bullet+}$)[33] and phenylacetylene ($C_6H_5CHCH_2^{\bullet+}$)[32] cations are summarized in Table 4. The DFT computed structures and the NBO charges for all three ions and the HCN molecule are shown in Figure 9. The DFT structures of the lowest energy two isomers of the $A^{\bullet+}(HCN)_n$ clusters for $A^{\bullet+}$ = $C_6H_5F^{\bullet+}$, $C_6H_4F_2^{\bullet+}$ and $C_6H_5CN^{\bullet+}$ are shown in Figures 8, 10, 11 and 12 for the clusters with n = 1, 2, 3 and 4, respectively. Additional optimized structures with their relative energies are given in the Supporting Information.

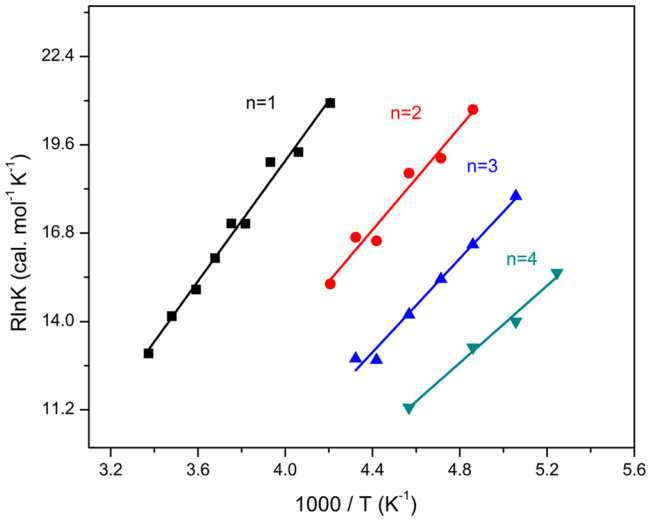

Figure 7. van't Hoff plots for the $C_6H_5CN^{\bullet+}(HCN)_{n-1}$ + HCN ⇌ $C_6H_5CN^{\bullet+}(HCN)_n$ association reactions for n = 1−4 as indicated.

Table 1. Measured and Computed Thermochemistry of the Stepwise Clustering Reactions of HCN Molecules with the $C_6H_5F^{\bullet+}$ Radical Cation[a]

n	$-\Delta H^\circ_{n-1,n}$	$-\Delta S^\circ_{n-1,n}$	$\Delta E_{n-1,n}$
1	11.2	24.4	9.6
2	9.0	21.8	8.5
3	8.7	24.6	7.9
4	7.8	25.1	7.4

[a]Units: ΔH° and ΔE (corrected for ZPE), kcal/mol; ΔS°, cal/(mol K). Error estimate for experimental values from standard deviations of van't Hoff and from usual uncertainties in clustering equilibrium temperature studies: ΔH°, ±1 kcal/mol; ΔS°, ±2 cal/(mol K).

Table 2. Measured Thermochemistry and Calculated Binding Energies of the Stepwise Clustering Reactions of HCN Molecules with the 1,4-$C_6H_5F^{\bullet+}$ Radical Cation[a]

n	$-\Delta H^\circ_{n-1,n}$	$-\Delta S^\circ_{n-1,n}$	$\Delta E_{n-1,n}$
1	11.2	22.5	9.8
2	9.3	21.1	8.6
3	8.2	21.6	7.9
4	7.7	22.3	7.3

[a]Units: ΔH° and ΔE (corrected for ZPE), kcal/mol; ΔS°, cal/(mol K). Error estimate for experimental values from standard deviations of van't Hoff and from usual uncertainties in clustering equilibrium temperature studies: ΔH°, ±1 kcal/mol; ΔS°, ±2 cal/(mol K).

Table 3. Measured Thermochemistry and Calculated Binding Energies of the Stepwise Clustering Reactions of HCN Molecules with the $C_6H_5CN^{\bullet+}$ Radical Cation[a]

n	$-\Delta H^\circ_{n-1,n}$	$-\Delta S^\circ_{n-1,n}$	$\Delta E_{n-1,n}$
1	9.6	19.1	9.5
2	8.2	19.0	8.5
3	7.4	19.6	7.6
4	6.1	16.6	7.3

[a]Units: ΔH° and ΔE (corrected for ZPE), kcal/mol; ΔS°, cal/(mol K). Error estimate for experimental values from standard deviations of van't Hoff and from usual uncertainties in clustering equilibrium temperature studies: ΔH°, ±1 kcal/mol; ΔS°, ±2 cal/(mol K).

dx.doi.org/10.1021/jp4069202 | J. Phys. Chem. A 2013, 117, 10588−10597

Table 4. Measured Association Enthalpies for the Stepwise Solvation of Radical Cations ($A^{\bullet+}$) by One to Four HCN Molecules (kcal/mol)

	$-\Delta H^\circ_{n-1,n}$ [$A^{\bullet+}(HCN)_n$]				
n	$C_6H_6^{\bullet+}$ [a]	$C_6H_5CN^{\bullet+}$	$C_6H_5CCH^{\bullet+}$ [b]	$C_6H_5F^{\bullet+}$	1,4-$C_6H_4F_2^{\bullet+}$
1	9.2	9.6	10.5	11.2	11.2
2	8.0	8.2	9.0	9.0	9.3
3	7.5	7.4	8.2	8.7	8.2
4	7.3	6.1	7.2	7.8	7.7

[a]Reference 33 [b]Reference 32.

4a. Addition of the First HCN Molecule. When theory and experiment are compared, the first HCN molecule binds to the fluorobenzene$^{\bullet+}$ and 1,4-difluorobenzene$^{\bullet+}$ radical cations with a measured binding energy of 11.2 ± 1 kcal/mol for both, and calculated binding energies of 9.6 and 9.9 kcal/mol, respectively. These binding energies show that the second fluorine substituent atom at the para position has no effect on the binding to the HCN molecule. This is also confirmed by the calculated DFT optimized lowest energy geometries of the ions, shown in Figure 8, which show that the first HCN molecule binds to the fluorobenzene radical cation at an angle of 87° to the plane of the fluorobenzene ion with a bond length of 2.8 Å, and similar geometries are observed with the difluorobenzene radical cation, with the ion plane-to-molecule angle and bond length of 88° and 2.9 Å, respectively. The ΔS° values are also similar within the experimental uncertainty of ±2 cal/(mol K), consistent with the energetic and structural similarities.

The experimentally measured binding energy of benzonitrile$^{\bullet+}$(HCN) of 9.6 kcal/mol is in excellent agreement with the calculated binding energy of 9.5 kcal/mol. The DFT optimized lowest energy geometry of the $C_6H_5CN^{\bullet+}$(HCN) cluster ion shows a bifurcated structure, with the HCN binding to two C−H hydrogen atoms by 2.7 and 2.4 Å bonds in the same plane, as shown in Figure 8. Hamid et al.[33] through experimental and theoretical investigations of benzene$^{\bullet+}$(HCN) and benzene$^{\bullet+}$(H_3CCN)[32] determined that these clusters have similar bifurcated structures as $C_6H_5CN^{\bullet+}$(HCN), and very similar ΔH° and ΔS° values.

The noncovalent adducts of HCN to the ionized aromatics are bonded primarily by electrostatic forces both in planar hydrogen-bonded structures and in vertical L-shaped structures in Figure 8. The electrostatic nature of the bonding is indicated by, for example, the transfer of only 0.035 charge from $C_6H_5F^{\bullet+}$ to the HCN ligand in Figure 8 (structure F1a). Although the results show comparable binding energies of HCN to all the ions, they result from different interactions with different charge centers.

With respect to the geometries of electrostatic (F1a) and hydrogen bonded isomers (F1b) shown in Figure 8, it appears that the bond length of the electrostatic C---N bond (2.8 Å) and C−H---N hydrogen bond (2.2 Å) bonds are significantly different, although the binding energies are nearly equal. However, the main interactions are between the positive benzene carbon atom and the negative nitrogen atom of the HCN molecule, and thus the overall carbon−nitrogen bond lengths are comparable in both isomers. In these terms, the C---N bond length in the electrostatic isomer (2.8 Å) and the C---N distance in the hydrogen bonded isomer [1.1 Å (C−H bond) + 2.2 Å (H---N) = 3.3 Å] are more comparable.

The atomic charges on the ions are also of interest. In fluorobenzene, the electronegative F atom is significantly negative and its carbon has a high partial positive charge (0.60) in the ion (Figure 9a). It appears that fluorine substitution creates a π hole at this carbon. The negative N end of the HCN neutral molecule (−0.31) (Figure 9d) can interact attractively with the large positive charge at this carbon, although this can be counterbalanced in part by repulsion with

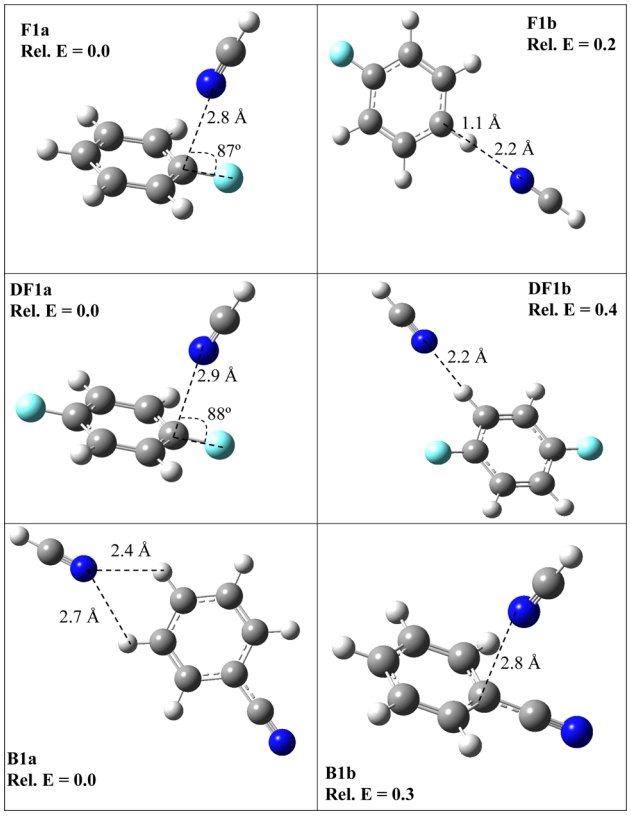

Figure 8. Selected DFT optimized structures for the $A^{\bullet+}$(HCN) cluster ions [A = $C_6H_5F^{\bullet+}$ (F), 1,4-$C_6H_4F_2^{\bullet+}$ (DF), or $C_6H_5CN^{\bullet+}$ (B)] showing the relative energies (Rel. E) in reference to the lowest computed energy isomer (a) given in Tables 1−3. Energies in kcal/mol.

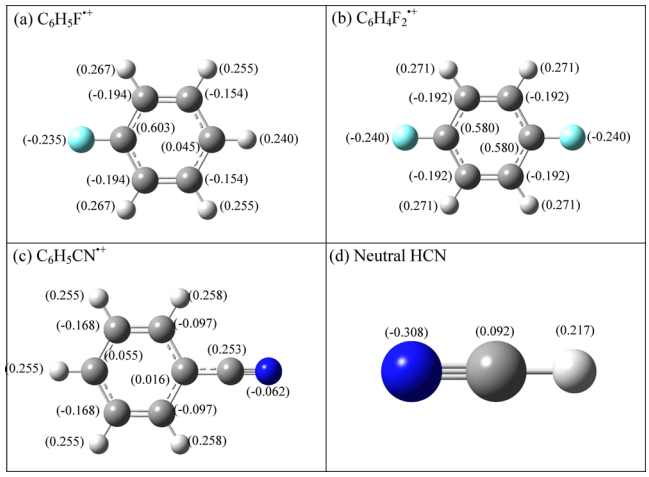

Figure 9. DFT computed natural bond orbital charges (NBO) at the B3LYP/6-311++G(d,p) level of theory for (a) fluorobenzene$^{\bullet+}$, (b) 1,4-difluorobenzene$^{\bullet+}$, (c) benzonitrile$^{\bullet+}$, and (d) HCN.

dx.doi.org/10.1021/jp4069202 | J. Phys. Chem. A 2013, 117, 10588−10597

the adjacent F atom (−0.24) and ortho carbons (−0.19) of the fluorobenzene cation (Figure 9a). On the other hand, in hydrogen bonding to the ring hydrogens, especially the para hydrogen, HCN interacts with a smaller positive charge (0.24), but this interaction is not destabilized by nearby negative charges. These effects balance out fortuitously to lead to practically equal binding energies in the planar and vertical isomers (Figure 8, isomers F1a and F1b). Similar charges, interactions, and binding energies apply in 1,4-difluorobenzene (see Figure 9b and isomers DF1a and DF1b in Figure 8). However, in benzonitrile$^{\bullet+}$, although the CN group is electron withdrawing, there are no large positive charges on the ring carbons (Figure 9c), and a planar bifurcated hydrogen-bonded structure has the lowest energy (isomer B1a, Figure 8) although a vertical electrostatic structure (isomer B1b, Figure 8) has a very similar energy, maybe somewhat fortuitously. This is basically similar to the case of benzene$^{\bullet+}$(HCN), which also has a lowest energy planar structure, as well as a vertical structure with HCN pointing to the center of the ring.[33] Moreover, despite the different charge distributions, interactions and structures, the binding energies of all of these systems are similar, within a small range of 9−11 kcal/mol.

4b. Addition of the Second HCN Molecule. In adding further solvent molecules, two types of clusters can be formed: *externally solvated* where the ligand molecules bind to each other and the ion is outside of the solvent cluster, and *internally solvated* clusters where the ligand molecules bind directly to the ion that is inside the solvent cluster. Mixed structures are also possible with several solvent molecules that can have both types of arrangements in one cluster. In the present clusters we observe all three types of structures (see Supporting Information).

The DFT optimized lowest energy geometries of the $C_6H_5F^{\bullet+}(HCN)_2$ and $C_6H_4F_2^{\bullet+}(HCN)_2$ clusters (structures F2a and DF2a, respectively, Figure 10) show that the second addition of HCN leads to the formation of an "externally solvated" structure where the second solvent molecule binds to the first, rather than binding directly to the ring structure of the ion. For $C_6H_5F^{\bullet+}(HCN)_2$ (structure F2a, Figure 10), the second HCN molecule binds to the first in the same plane a bond length of 2.1 Å. The bond length between the aromatic ring and the first HCN is also reduced upon the second HCN binding. Similar results are obtained for the 1,4-$C_6H_4F_2^{\bullet+}(HCN)_2$ (structures DF2a and DF2b, which have practically equal energies, Figure 10). Further, the measured binding energies of the second HCN to the $C_6H_5F^{\bullet+}(HCN)$ and $C_6H_4F_2^{\bullet+}(HCN)$ ions in Tables 1 and 2 are similar both in experiment and in theory. The measured BDE for $n = 2$ are 9.0 and 9.3 kcal/mol for $C_6H_5F^{\bullet+}(HCN)_n$ and 1,4-$C_6H_4F_2^{\bullet+}(HCN)_n$, respectively, which agree well with the calculated ΔE° values of 8.5 and 8.6 kcal/mol, respectively. On the basis of these observations, the B3LYP/6-311++G (d,p) level of theory yielded satisfactory results for the present systems.

For the second addition of HCN molecule onto the $C_6H_5CN^{\bullet+}(HCN)$ cluster we observe 8.2 and 8.5 kcal/mol as the experimentally measured and theoretically calculated binding energies, respectively (Table 3), which are in excellent agreement. Unlike the second addition of HCN to $C_6H_5F^{\bullet+}(HCN)$ and $C_6H_4F_2^{\bullet+}(HCN)$, which leads to externally solvated complexes, the second addition of HCN to the $C_6H_5CN^{\bullet+}(HCN)$ cluster ion binds directly to a C−H hydrogen at the meta position on the aromatic ring of the

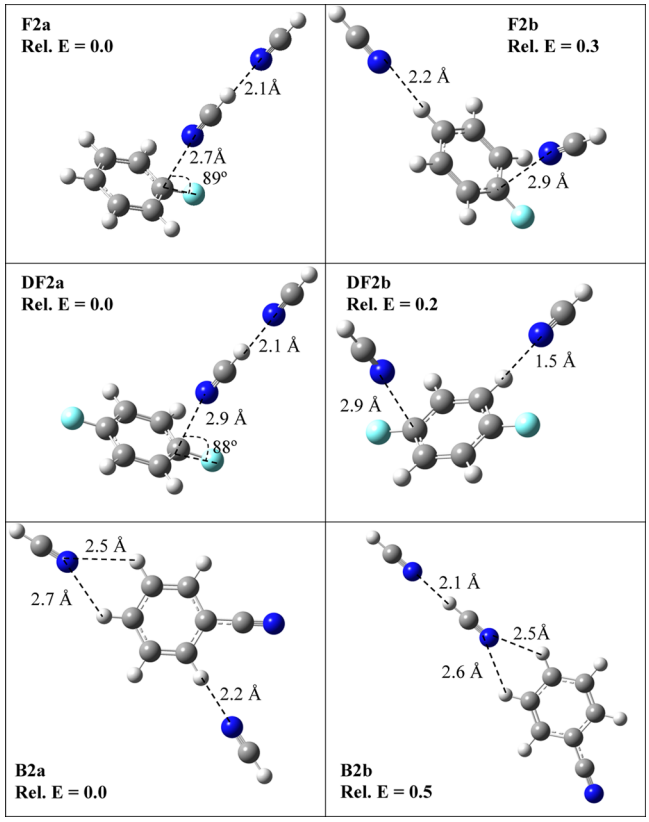

Figure 10. Selected DFT optimized structures for the $A^{\bullet+}(HCN)_2$ cluster ions [A = $C_6H_5F^{\bullet+}$ (F), 1,4-$C_6H_4F_2^{\bullet+}$ (DF), or $C_6H_5CN^{\bullet+}$ (B)] showing the relative energies (Rel. E) in reference to the lowest computed energy isomers (a) given in Tables 1−3. Energies in kcal/mol.

$C_6H_5CN^{\bullet+}$ ion with a bond length of 2.2 Å (structure B2a, Figure 10). Comparing the experimentally measured and theoretically computed binding energies in Tables 1−3 for the second addition of the HCN ligand to all the three ions shows similar bond strengths between the $A^{\bullet+}(HCN)$ ions and the second HCN ligand, even though $C_6H_5F^{\bullet+}(HCN)$ and $C_6H_4F_2^{\bullet+}(HCN)$ form externally solvated complex ions, whereas $C_6H_5CN^{\bullet+}(HCN)$ forms an internally solvated complex ion. Previous studies in ionized aromatic clusters with HCN also found similar experimental and theoretical binding energies for the second addition of HCN to the $A^{\bullet+}(HCN)$ cluster ion as 8.0 kcal/mol (exp) and 8.2 kcal/mol (calc) for the benzene radical cation, and 9.0 kcal/mol (exp) and 7.6 kcal/mol (calc) for the phenylacetylene radical cation.[32,33] These binding energies follow the common trend of decreasing binding energies of consecutive ligand molecules to cluster ions due to the increasing charge delocalization in the cluster and consequently, decreasing charge at the binding sites.

These observations suggest that after the first HCN ligand, the influence of the molecular ion on the strength of the bond formed between the $A^{\bullet+}(HCN)$ and the incoming HCN ligand is reduced, and it depends more on the nature of the incoming ligand. Hamid et al.[33] found the second acetonitrile ligand bound to the $C_6H_6^{\bullet+}(NCCH_3)$ cluster ion with a binding energy of 10.7 kcal/mol, whereas Ibrahim et al.[27,28] found the binding energy of a second H_2O molecule to $C_6H_6^{\bullet+}(H_2O)$ to be 8.0 kcal/mol. This trend validates the conclusion reached by Hamid et al. that ligands with higher dipole moments will bind more strongly to the $A^{\bullet+}(X)$ [X = HCN, CH_3CN, H_2O, etc.]

dx.doi.org/10.1021/jp4069202 | J. Phys. Chem. A 2013, 117, 10588−10597

with less dependence on the identity of the core ions. This could suggest that most of the rearrangement of the charge density of the molecular ion due to adding a ligand occurs after the first addition, whereas the second addition only alters the charge distribution minimally and has little influence on the effective binding energy.

4c. Addition of the Third HCN Molecule. The third HCN in $C_6H_5F^{\bullet+}(HCN)_3$ and 1,4-$C_6H_4F_2^{\bullet+}(HCN)_3$ binds directly to ring hydrogens, forming structures with elements of both internally and externally solvated cluster ions (structures F3a and DF3a, respectively, Figure 11). In the

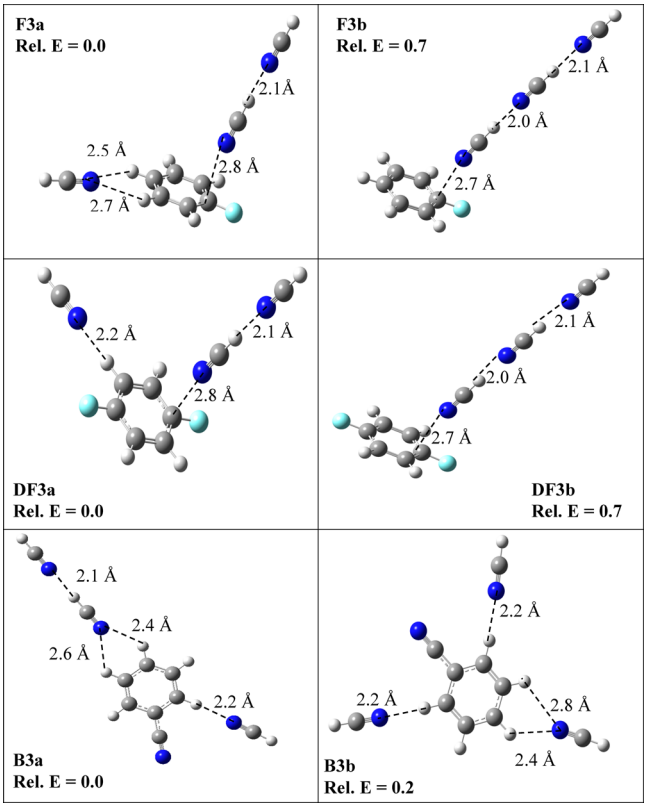

Figure 11. Selected DFT optimized structures for the $A^{\bullet+}(HCN)_3$ cluster ions [A = $C_6H_5F^{\bullet+}$ (F), 1,4-$C_6H_4F_2^{\bullet+}$ (DF), or $C_6H_5CN^{\bullet+}$ (B)] showing the relative energies (Rel. E) in reference to the lowest computed energy isomers (a) given in Tables 1−3. Energies in kcal/mol.

$C_6H_5F^{\bullet+}(HCN)_3$ cluster (F3a isomer, Figure 11), the third HCN molecule forms a bifurcated structure with the two C−H hydrogens at the meta and para positions of the aromatic ring, whereas in 1,4-$C_6H_4F_2^{\bullet+}(HCN)_3$ the incoming HCN binds to the C−H hydrogen at the meta position with respect to the first HCN molecule on the aromatic ring (isomer DF3a, Figure 11). It should be noted that several structures that combine both internally and externally solvated features exist with practically the same energy as that of structure DF3a (see structures DF3b, DF3c, and DF3d, Supporting Information). In the case of $C_6H_5CN^{\bullet+}(HCN)_3$, the third HCN binds to the first HCN *externally* (isomer B3a, Figure 11). The measured binding energies for the third addition of HCN unto the three aromatic ions agree excellently with the calculated values, as shown in Tables 1−3. The binding energy of the third addition is still slightly higher for $C_6H_5F^{\bullet+}(HCN)_3$ (8.7 kcal/mol) and 1,4-$C_6H_4F_2^{\bullet+}(HCN)_3$ (8.2 kcal/mol) than for $C_6H_5CN^{\bullet+}(HCN)_3$ (7.4 kcal/mol).

4d. Addition of the Fourth HCN Molecule. In the $C_6H_5F^{\bullet+}(HCN)_4$ cluster, the fourth HCN binds externally to the third bifurcated HCN with a bond length of 2.1 Å (structure F4a, Figure.12). The measured binding energy for this addition is 7.8 kcal/mol, in good agreement with the DFT calculated value of 7.4 kcal/mol. The fourth HCN in $C_6H_4F_2^{\bullet+}(HCN)_4$ binds externally to the second meta position on the aromatic ring, as shown in Figure 12 (structure DF4a),

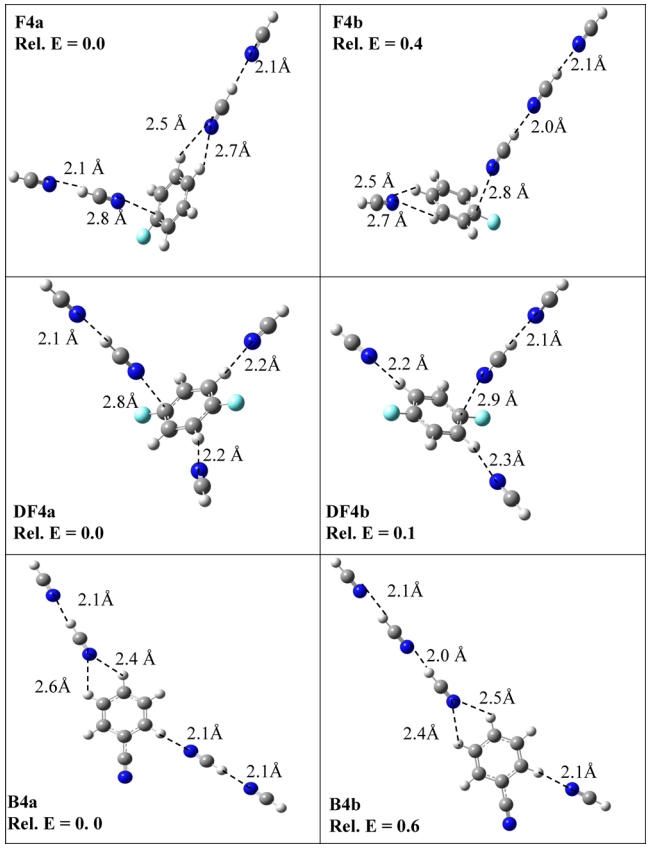

Figure 12. Selected DFT optimized structures for the $A^{\bullet+}(HCN)_4$ cluster ions [A = $C_6H_5F^{\bullet+}$ (F), 1,4-$C_6H_4F_2^{\bullet+}$ (DF), or $C_6H_5CN^{\bullet+}$ (B)] showing the relative energies (Rel. E) in reference to the lowest computed energy isomers (a) given in Tables 1−3. Energies in kcal/mol.

with a bond length of 2.2 Å. The measured binding energy of 7.7 kcal/mol agrees well with the theoretical value of 7.3 kcal/mol. In the benzonitrile cluster ion $C_6H_5CN^{\bullet+}(HCN)_4$, the fourth HCN ligand binds externally to the HCN at the ortho position, with a bond length of 2.1 Å (structure B4a, Figure 12). Again, several structures that combine both internally and externally solvated features exist for the $C_6H_5CN^{\bullet+}(HCN)_4$ cluster within 0.6 kcal/mol of the energy of the B4a structure (see structures B4b, B4c and B4d, Supporting Information). The measured binding energy for this addition is 6.1 kcal/mol, which is lower than the DFT binding energy of the lowest energy isomer (B4a, Figure 12) of 7.3 kcal/mol, but within the experimental uncertainty range of ±1 kcal/mol for clustering equilibrium temperature studies. As in all such clusters,[1] the binding energies converge to the enthalpy of vaporization of the ligand (ΔH°_{vap}), which is 6.0 kcal/mol for HCN at 298 K.[38]

dx.doi.org/10.1021/jp4069202 | J. Phys. Chem. A 2013, 117, 10588−10597

5. SUMMARY AND CONCLUSIONS

The thermochemistry of the stepwise solvation of the radical cations fluorobenzene, 1,4-difluorobenzene, and benzonitrile by one to four HCN molecules was measured using ion mobility mass spectrometry and DFT calculations and was compared with the corresponding thermochemistry of ionized benzene and phenylacetylene measured in previous studies.[32,33] Compared with $C_6H_6^{\bullet+}(HCN)_n$ clusters, the electron-withdrawing substituents increase slightly the ligand binding energies due to larger positive charges on the hydrogen bonding aromatic CH hydrogens, and in fluorobenzenes, by creating high positive charges or π holes on the fluorinated carbons. However, the binding energies of an HCN molecule to all five ionized benzene derivatives are similar, between 9.2 and 11.2 kcal/mol. The HCN ligand can form linear or bifurcated C−H---N ionic hydrogen bonds to all of the ions studied. With fluorobenzenes, it can form a vertical L-shaped geometry by bonding electrostatically to a positive charge center or π hole on the fluorinated carbon, but this attractive force is partially counterbalanced by repulsive interactions with the adjacent negative charges on fluorine and the ortho carbons. As a result, the in-plane hydrogen bonded and out-of-plane vertical structures have, fortuitously, nearly equal energies. With the other ionized aromatics the in-plane hydrogen bonded structures have lower energies, although stable vertical adducts are also available.

All the calculated lowest energy geometry isomers have computed bond lengths of the aromatic ring to HCN of more than 2.0 Å, indicating that no covalent bonds are being observed, consistent with the experimental binding energies below 11.2 kcal/mol.

In higher clusters with two to four HCN molecules, the further ligand molecules can hydrogen bond to the core ions, or add to the first ligand molecules to form linear HCN---HCN---HCN chains hydrogen bonded to the core ions. With three to four HCN molecules both structural types can be found in the same cluster. In general, isomers with various structural types often have energies within 1 kcal/mol. Therefore, the observed populations at thermal energies should contain equilibrium mixtures of these isomers.

Together with previous studies, these results show that ionized aromatics can form several different types of complexes with polar molecules including in-plane internally or externally solvated hydrogen-bonded structures or electrostatic out-of-plane complexes. Each type may be affected by substituents or fused ring substitutions on the ionized aromatics, but the substituent effects are small, and they are comparable for electrostatic and hydrogen-bonded isomers. Therefore, the energies of electrostatic and hydrogen-bonded isomers remain comparable in all of the systems studied.

■ ASSOCIATED CONTENT

Supporting Information

DFT optimized structures for different isomers of the HCN clusters (one to four molecules) with the radical cations fluorobenzene$^{\bullet+}$, 1,4-difluorobenzene$^{\bullet+}$, and benzonitrile$^{\bullet+}$ calculated at the B3LYP/6-311++G(d,p) level. This material is available free of charge via the Internet at http://pubs.acs.org

■ AUTHOR INFORMATION

Notes

The authors declare no competing financial interest.

■ ACKNOWLEDGMENTS

We thank the National Science Foundation (CHE-0911146) and NASA (NNX07AU16G) for the support of this work. The authors are grateful to King Abdulaziz University for the partial support of this work.

■ REFERENCES

(1) Meot-Ner (Mautner), M. *Chem. Rev.* **2012**, *112*, PR22−103.
(2) Cerny, J.; Hobza, P. *Phys. Chem. Chem. Phys.* **2007**, *9*, 5291.
(3) Jeffrey, G. A. *An Introduction to Hydrogen Bonding*; Oxford University press: Oxford, U.K., 1997.
(4) Conway, B. E. *Ionic Hydration in Chemistry and Biophysics*; Elsevier: Amsterdam, New York, 1981.
(5) Tsuzuki, S. In *Intermolecular Forces and Clusters I*; Wales, D. J., Ed.; Springer: Berlin, Heidelberg: 2005; Vol. *115*, p 149.
(6) Menor-Salvan, C.; Marin-Yaseli, M. R. *Chem. Soc. Rev.* **2012**, *41*, 5404−5415.
(7) Garand, E.; Kamrath, M. Z.; Jordan, P. A.; Wolk, A. B.; Leavitt, C. M.; McCoy, A. B.; Miller, S. J.; Johnson, M. A. *Science* **2012**, *335*, 694.
(8) Tarakeshwar, P.; Kim, K. S.; Brutschy, B. *J. Chem. Phys.* **1999**, *110*, 8501.
(9) Nuevo, M.; Milam, S. N.; Sandford, S. A.; Elsila, J. E.; Dworkin, J. P. *Astrobiology* **2009**, *9*, 683−695.
(10) Tsuzuki, S.; Fujii, A. *Phys. Chem. Chem. Phys.* **2008**, *10*, 2584.
(11) Sloan, E. D. M. D. *Clathrate Hydrates of Natural Gases*; CRC Press: Boca Raton, FL, 2008; Vol. *3*.
(12) Ben-Naim, A. *Hydrophobic Interactions*; Plenum: New York, 1980.
(13) Dougherty, D. A. *Science* **1996**, *271*, 163.
(14) Ugozzoli, F. A., A.; Massera, C.; Pochini, A.; Secchi, A. *New J. Chem.* **2002**, *26*, 1718.
(15) Meot-Ner (Mautner), M.; Hamlet, P.; Hunter, E. P.; Field, F. H. *J. Am. Chem. Soc.* **1978**, *100*, 5466.
(16) Meot-Ner (Mautner), M. *J. Phys. Chem.* **1980**, *84*, 2724.
(17) Meot-Ner (Mautner), M. *Acc. Chem. Res.* **1984**, *17*, 186.
(18) Meot-Ner (Mautner), M.; El-Shall, M. S. *J. Am. Chem. Soc.* **1986**, *108*, 4386.
(19) El-Shall, M. S.; Kafafi, S. A.; Meot-Ner (Mautner), M.; Kertesz, M. *J. Am. Chem. Soc.* **1986**, *108*, 4391.
(20) El-Shall, M. S.; Meot-Ner (Mautner), M. *J. Phys. Chem.* **1987**, *91*, 1088.
(21) Rusyniak, M. J.; Ibrahim, Y. M.; Wright, D. L.; Khanna, S. N.; El-Shall, M. S. *J. Am. Chem. Soc.* **2003**, *125*, 12001.
(22) Rusyniak, M.; Ibrahim, Y.; Alsharaeh, E.; Meot-Ner (Mautner), M.; El-Shall, M. S. *J. Phys. Chem. A* **2003**, *107*, 7656.
(23) Pieniazek, P. A.; Krylov, A. I.; Bradforth, S. E. *J. Chem. Phys.* **2007**, *127*, 044317.
(24) Pieniazek, P. A.; Bradforth, S. E.; Krylov, A. I. *J. Chem. Phys.* **2008**, *129*, 074104.
(25) Sinnokrot, M. O.; Sherrill, C. D. *J. Phys. Chem. A* **2006**, *110*, 10656.
(26) Podeszwa, R.; Bukowski; Szalewicz, K. *J. Phys. Chem. A* **2006**, *110*, 10345.
(27) Ibrahim, Y.; Alsharaeh, E.; Dias, K.; Meot-Ner, M.; El-Shall, M. S. *J. Am. Chem. Soc.* **2004**, *127*, 12766−12767.
(28) Ibrahim, Y.; Alsharaeh, E.; Meot-Ner, M.; El-Shall, M. S.; Scheiner, S. *J. Am. Chem. Soc.* **2005**, *127*, 7053−7064.
(29) Ibrahim, Y.; Mabrouki, R.; Meot-Ner, M.; El-Shall, M. S. *J. Phys. Chem. A.* **2007**, *111*, 1006−1014.
(30) Momoh, P. O.; El-Shall, M. S. *Chem. Phys. Lett.* **2007**, *436*, 25−29.
(31) Momoh, P. O.; El-Shall, M. S. *Phys. Chem. Chem. Phys.* **2008**, *10*, 4827−4834.
(32) Hamid, A. M.; Soliman, A.-R.; El-Shall, M. S. *Chem. Phys. Lett.* **2012**, *543*, 23.
(33) Hamid, A. M.; Soliman, A. R.; El-Shall, M. S. *J. Phys. Chem. A* **2013**, *117*, 1069.

(34) El-Shall, M. S.; Ibrahim, Y. M.; Alsharaeh, E. H.; Meot-Ner (Mautner), M.; Watson, S. P. *J. Am. Chem. Soc.* **2009**, *131*, 10066.
(35) Meot-Ner (Mautner), M. *J. Am. Chem. Soc.* **1978**, *100*, 4694.
(36) Meot-Ner (Mautner), M.; Karpas, Z.; Deakyne, C. A. *J. Am. Chem. Soc.* **1986**, *108*, 3193.
(37) Frisch, M. J.; Trucks, G. W.; Schlegel, H. B.; Scuseria, G. E.; Robb, M. A.; Cheeseman, J. R.; Zakrzewski, V. G.; Montgomery, J. A.; Stratmann, R. E.; Burant, J. C.; et al. *Gaussian 03*, revision C.02; Gaussian, Inc.: Pittsburgh, PA, 2004.
(38) Linstrom, P. J., Mallard, W. G., Eds. *NIST Chemistry WebBook*; NIST Standard Reference Database Number 69; National Institute of Standards and Technology: Gaithersburg MD, 20899, http://webbook.nist.gov.